

# A numerical study of the pull-in instability in some free boundary models for MEMS

Gilberto Flores,  
Instituto de Investigaciones en Matemáticas Aplicadas y en Sistemas,  
and FENOMECE  
Universidad Nacional Autónoma de México,  
Apdo. Postal 20-126,  
01000 México, D.F., MEXICO  
(gfg@mym.iimas.unam.mx)

Noel F. Smyth,  
School of Mathematics,  
University of Edinburgh,  
Edinburgh, Scotland, U.K., EH9 3FD.  
(N.Smyth@ed.ac.uk)

## Abstract

In this work we numerically compute the bifurcation curve of stationary solutions for the free boundary problem for MEMS in one space dimension. It has a single turning point, as in the case of the small aspect ratio limit. We also find a threshold for the existence of global-in-time solutions of the evolution equation given by either a heat or a damped wave equation. This threshold is what we term the dynamical pull-in value: it separates the stable operation regime from the touchdown regime. The numerical calculations show that the dynamical threshold values for the heat equation coincide with the static values. For the damped wave equation the dynamical threshold values are smaller than the static values. This result is in agreement with the observations reported for a mass-spring system studied in the engineering literature. In the case of the damped wave equation, we also show that the aspect ratio of the device is more important than the inertia in the determination of the pull-in value.

Key words: Quenching, MEMS, damped wave equation, parabolic equation, free boundary.

## 1. Introduction

The operation of many micro electromechanical systems (MEMS) relies upon the action of electrostatic forces. Many such devices, including pumps, switches or valves, can be modelled by electrostatically deflected elastic membranes. Typically a MEMS device consists of an elastic membrane held at a constant voltage and suspended above a rigid ground plate placed in series with a fixed voltage source. The voltage difference causes a deflection of the membrane, which in turn generates an electric field in the region between the plate and the membrane. Mathematically, this is then a free boundary problem. The electric potential is defined in a region which depends on the membrane deflection, while the elastic deformation is forced by the trace of the electric field on the membrane.

An important nonlinear phenomenon in electrostatically deflected membranes is the so-called “pull-in” instability. For moderate voltages the system is in the stable operation regime: the membrane approaches a steady state and remains separate from the ground plate. When the voltage is increased beyond a critical value, there is no longer an equilibrium configuration of the membrane. As a result, the membrane collapses onto the ground plate. This phenomenon is also known as “touchdown”. The critical value of the voltage required for touchdown to occur is termed the *pull-in value*. The determination of the pull-in value is important for the design and manufacture of MEMS devices, particularly as touchdown is a desirable property in devices such as microvalves. For instance, Desai *et al* [1] give a description of microvalves used in microfluidic chips. However, for most devices, it is desirable to achieve the stable operation regime with no touchdown. The *pull-in distance* is the critical distance between the ground plate and the elastic membrane beyond which pull-in occurs.

The issue of the static and dynamical pull-in instabilities has been addressed by the engineering community in the context of a model in which the moving structure is a plate attached to a spring with damping. The elastic properties of the moving plate are described by the restoring force of the spring, which is assumed to be given by Hooke’s law. The voltage applied to the moving plate results in an electrostatic force acting on the spring-mass system, see Rocha *et al* [2] and Zhang *et al* [3] for details. The governing equation for the displacement of the moving mass is

$$m\frac{d^2x}{dt^2} + b\frac{dx}{dt} + kx = \frac{\lambda}{(d_0 - x)^2}, \quad (1)$$

where  $d_0$  is the initial gap between the plates,  $\lambda = \epsilon_0 AV^2/2$ ,  $A$  is the area of the moving plate,  $V$  is the voltage applied to it and  $\epsilon_0$  is the permittivity of the free space between the plates. The right hand side is the Coulomb force.

Zhang *et al* [3] described the dynamical pull-in as the collapse of the moving structure towards the substrate due to the combined action of kinetic and potential energies. They also stated that, in general, **dynamical pull-in requires a lower voltage to be triggered compared to the static pull-in threshold**. One of the findings in Rocha *et al.* [2] is the fact that for an overdamped device, the dynamics in the touchdown regime has three distinguished regions characterized by different time scales: in the first region the structure moves fast until it gets near the static pull-in distance, at which point there is a metastable region in which the motion is very slow, and finally a third region in which collapse takes place on a fast time scale.

In the present work we study the equations obtained when the deflection of the elastic membrane is governed by a forced, damped wave equation. We also study the forced heat equation which corresponds to setting the inertia equal to zero. For simplicity, we assume that the motion starts from rest. The numerical results indicate that for the forced heat equation, the dynamical pull-in value coincides with the static value. This result is supported by the fact that the membrane profiles decrease monotonically in time and approach a steady state in the stable operation regime, which suggests that there is a maximum principle and that the stationary solutions act as a barrier to prevent touchdown. This is exactly the situation in the limit of vanishing aspect ratio. In contrast, the dynamical pull-in value for the damped wave equation is smaller than the static value, in agreement with the observation in [3] for equation (1). We also obtain the different time scales in the dynamics of touchdown as reported in [2] for equation (1). Our results then indicate that the difference between the dynamical and static pull-in values is due to the inertial forces. On the other hand, our calculations show that the aspect ratio is more important than the inertia in the determination of the dynamical pull-in value.

Here we study the following free-boundary problem. Let  $u$  denote the membrane deformation. In terms of dimensionless variables, the electric potential  $\psi$  is defined in the region

$$\Omega(u) = \{(x, z) \in (-1, 1) \times (-1, \infty) : -1 < z < u(x)\}. \quad (2)$$

The electric potential itself is the solution of the elliptic equation

$$\epsilon^2 \psi_{xx} + \psi_{zz} = 0 \quad (3)$$

together with the boundary conditions

$$\psi(x, -1) = 0, \quad \psi(x, u(x)) = 1 \text{ for } x \in (-1, 1), \quad \psi(\pm 1, z) = 1 + z \text{ for } z \in (-1, 0). \quad (4)$$

The membrane deformation  $u$  itself is the solution of

$$\gamma u_{tt} + u_t - u_{xx} = -\lambda [\epsilon^2 |\psi_x(x, u(x))|^2 + |\psi_z(x, u(x))|^2]. \quad (5)$$

For simplicity, we assume that the motion starts from the rest position. In these equations, the control parameter  $\lambda$  is proportional to the square of the applied voltage,  $\epsilon$  is the ratio of the gap size to the device length and  $\gamma$  is the ratio of inertial to damping forces. For a derivation of these equations see Pelesko and Bernstein [4].

In the formulation above there are other effects which have not been included. One is the effect of the electric field at the edge of the membrane, known as *fringing fields*. In addition, the elastic energy in the present model does not include the curvature of the membrane. Pelesko and Driscoll [6] gave a derivation of the governing equation when the fringing field is taken into account. The boundary value problem for the electric potential (3)–(4) is then solved for  $\epsilon = 0$  with a boundary layer correction around the edge of the membrane. Brubaker and Pelesko [7] studied the case in which the elastic energy includes the curvature of the membrane. The electric potential is obtained for  $\epsilon = 0$ .

The small aspect ratio limiting case corresponding to  $\epsilon = 0$  has been studied extensively. In this case, the boundary value problem (3) and (4) for the electric potential can be solved explicitly to give

$$\psi(x, z) = \frac{1 + z}{1 + u(x)}, \quad (x, z) \in \Omega(u). \quad (6)$$

Equation (5) for the elastic deformation then reduces to a nonlinear wave equation, termed the small aspect ratio model

$$\gamma u_{tt} + u_t - u_{xx} = -\frac{\lambda}{(1 + u)^2}. \quad (7)$$

The further limiting case with  $\gamma = 0$  is a nonlinear heat equation for which the dynamical pull-in value coincides with the critical value  $\lambda^*$  for the existence of stationary solutions of (7). Indeed, there are two, one or zero stationary solutions of (7) according to whether  $\lambda < \lambda^*$ ,  $\lambda = \lambda^*$  or  $\lambda > \lambda^*$ . Moreover, solutions of the nonlinear heat equation corresponding to  $\lambda \leq \lambda^*$  converge to a steady state, while solutions corresponding to  $\lambda > \lambda^*$  quench in finite time. The proof of this behaviour relies on the maximum principle, see Flores *et al* [5].

The same behaviour is obtained when the effect of fringing fields is taken into account. According to Pelesko and Driscoll [6], equation (7) is modified as follows. The numerator on the right hand side becomes  $-\lambda(1 + \epsilon^2 u_x^2)$ . For stationary solutions,

Lindsay and Ward [8] have established that the pull-in value  $\lambda^*(\epsilon)$  admits an asymptotic expansion in powers of  $\epsilon^2$  and obtained the leading order term, which in the one-dimensional case corresponds to the critical value  $\lambda^*$  mentioned in the previous paragraph. Wei and Ye [9] have described the structure of the stationary solutions for this problem. There is a critical value of  $\lambda$  such that there are at least two solutions, one or none according to whether  $\lambda$  is smaller, equal to, or larger than this critical value. Liu and Wang [10] verified that for the corresponding heat equation, the dynamical critical parameter coincides with the static critical value. The stationary solution thus acts as a barrier and prevents touchdown. The rule is that the static and dynamical pull-in values coincide whenever there is a maximum principle.

On the other hand, the numerical evidence for the case  $\gamma > 0$  indicates that for the damped wave equation (7) there is a threshold, which we denote by  $\lambda_w^*$ , that separates the stable operation regime from the touchdown regime. This means that solutions of (7) converge to a steady state for  $\lambda < \lambda_w^*$ , while for  $\lambda > \lambda_w^*$  solutions quench in finite time. This critical value of  $\lambda$  is what we call the *dynamical pull-in value*. Moreover,  $\lambda_w^* < \lambda^*$ , see Flores [11]. Similar numerical results concerning the dynamical threshold were obtained for conservative wave equations with a singular forcing term in one dimension by Chang and Levine [12] and in higher dimensions by Smith [13]. In the same context, Kavallaris *et al* [14] numerically found the existence of a dynamical threshold, smaller than the static value, in a one dimensional, non-local version of the equation considered in [12] for which the MEMS device is connected in series with a capacitor.

The experimental investigation of Siddique *et al* [15] points in the same direction. They set up an array of two plates, one fixed, the other with a laser cut hole where a soap film was applied. The plates were separated by a distance  $d$ . The critical voltage was computed for different values of  $d$ . An empirical relation was then used to determine the critical value of  $\lambda$ . These values were compared with either upper and lower bounds or with numerically computed values of  $\lambda^*$  for elliptical or rectangular domains. Good agreement was found for small values of  $d$ . It was found that the experimental values were smaller than the numerically calculated values. The interpretation of this is that the experimental values correspond to the dynamical critical value of  $\lambda$ . In Siddique *et al.* [15] a question is raised so as to identify the most important effect which accounts for the difference between the theoretical and the experimental results. The numerical results of the present work indicate that the aspect ratio of the device is more important than the inertial effects. Another part of the explanation is that the static and dynamical pull-in values are different.

The static free boundary problem and the associated semilinear parabolic equation in

one space dimension governing it have been analyzed by Laurençot *et al* [16] and by Escher *et al* [17], respectively. In the first work the existence of stationary solutions for small values of  $\lambda$  was established, as well as the non-existence for large values of this control parameter. The local well-posedness of the parabolic problem was proved in [17]. It was also established that for small values of  $\lambda$  the solution exists for all times and converges to a steady state as  $t \rightarrow \infty$ . It was also proved that for large values of  $\lambda$  global existence does not hold in the sense that  $u$  reaches the value  $-1$  in finite time, that is,  $u$  *quenches* in finite time. To the best of our knowledge these are the only rigorous results to date for the free boundary problem. As mentioned in Laurençot *et al* [16], no further information is available on the structure of the set of values of  $\lambda$  for which there is a classical stationary solution of the free boundary problem. It is believed that this set is an interval. In the present work, by computing the bifurcation curve we provide numerical evidence that this is indeed the case. The shape of the bifurcation curve for the steady states is qualitatively similar to the corresponding curve for the small aspect ratio limit corresponding to  $\epsilon = 0$ , which suggests the existence of a critical value  $\lambda^*(\epsilon)$  for a steady state to exist. The numerical results also indicate that  $\lambda^*(\epsilon) \rightarrow \lambda^*$  as  $\epsilon \rightarrow 0^+$ .

We also provide numerical evidence which shows that this static critical value  $\lambda^*(\epsilon)$  coincides with the dynamical pull-in value for the nonlinear heat equation. In contrast, for the damped wave equation it does not control the dynamics since the dynamic pull-in value is smaller than the static critical value, even in the limiting case  $\epsilon = 0$ . Therefore, the difference between the dynamic and static critical values is due to the inertial forces. We also find that the aspect ratio  $\epsilon$  is more important than the inertia coefficient  $\gamma$  in the determination of the dynamical pull-in value.

## 1 Stationary solutions

As discussed in the previous section, the equation for the electric potential  $\psi$  is

$$\epsilon^2 \psi_{xx} + \psi_{zz} = 0 \tag{8}$$

in the region  $\Omega(u) = \{(x, z) \in (-1, 1) \times (-1, \infty) : -1 < z < u(x)\}$ , together with the boundary conditions

$$\psi(x, -1) = 0, \quad \psi(x, u(x)) = 1 \text{ for } x \in (-1, 1), \quad \psi(\pm 1, z) = 1+z \text{ for } z \in (-1, 0). \tag{9}$$

The elastic deformation  $u$  is the solution of

$$u_{xx} = \lambda [\epsilon^2 |\psi_x(x, u(x))|^2 + |\psi_z(x, u(x))|^2] \tag{10}$$

with the boundary condition  $u(\pm 1) = 0$ .

Following Laurençot *et al* [16], we map the domain  $\Omega(u)$  onto the rectangle

$$\Omega = (-1, 1) \times (0, 1) \quad (11)$$

by means of the transformation

$$T_u(x, z) = \left( x, \frac{1+z}{1+u(x)} \right), \quad (12)$$

which has the inverse

$$T_u^{-1}(x, \eta) = (x, [1+u(x)]\eta - 1). \quad (13)$$

In terms of the new independent variables  $(x, \eta)$ , the electric potential is denoted by  $\phi$ :  $\phi = \psi \circ T_u^{-1}$ . The potential equation (8) then becomes

$$\mathcal{L}_u(\phi) = 0 \quad \text{in } \Omega, \quad \phi(x, \eta) = \eta \quad \text{on } \partial\Omega, \quad (14)$$

where  $\mathcal{L}_u$  is the elliptic operator defined by

$$\mathcal{L}_u(\phi) = \epsilon^2 \phi_{xx} - 2\epsilon^2 \eta \frac{u_x}{1+u(x)} \phi_{x\eta} + \frac{1+\epsilon^2 \eta^2 u_x^2}{[1+u(x)]^2} \phi_{\eta\eta} + \epsilon^2 \eta \left[ 2 \left( \frac{u_x}{1+u(x)} \right)^2 - \frac{u_{xx}}{1+u(x)} \right] \phi_\eta. \quad (15)$$

Equation (10) for the elastic deformation  $u$  becomes

$$u_{xx} = \lambda \left[ \frac{1+\epsilon^2 u_x^2}{(1+u(x))^2} \right] |\phi_\eta(x, 1)|^2 \quad (16)$$

in  $(-1, 1)$ , with the boundary condition  $u(\pm 1) = 0$ .

The transformed potential and elastic equations (14) and (16) were solved numerically using centred finite differences for the derivatives, so that the errors are  $O(\Delta x^2, \Delta \eta^2)$ . The potential equation (14) then becomes a linear system in  $\phi$  which was solved using Jacobi iteration. The elastic equation (16) is a nonlinear two point boundary value problem and was solved using a shooting method. The potential equation (14) and the elastic equation (16) form a coupled system due to  $u$  appearing in the elliptic operator (15). A Picard iteration was then used to solve this coupled system. A starting guess for  $\phi_\eta(x, 1)$  was assumed and then the elliptic equation (14) was solved to find  $\phi$  and so  $\phi_\eta$  at  $\eta = 1$ . The deformation equation (16) was then solved for  $u$  using this  $\phi_\eta(x, 1)$ . With this updated  $u(x)$  the elliptic equation (14) was again solved and the process iterated until convergence. The numerical results show the existence of a critical value of  $\lambda$ , denoted by  $\lambda_s^*(\epsilon)$ , such that there are two, one or zero stationary solutions according to whether  $\lambda$  is below, equal to or above the critical value  $\lambda_s^*(\epsilon)$ .

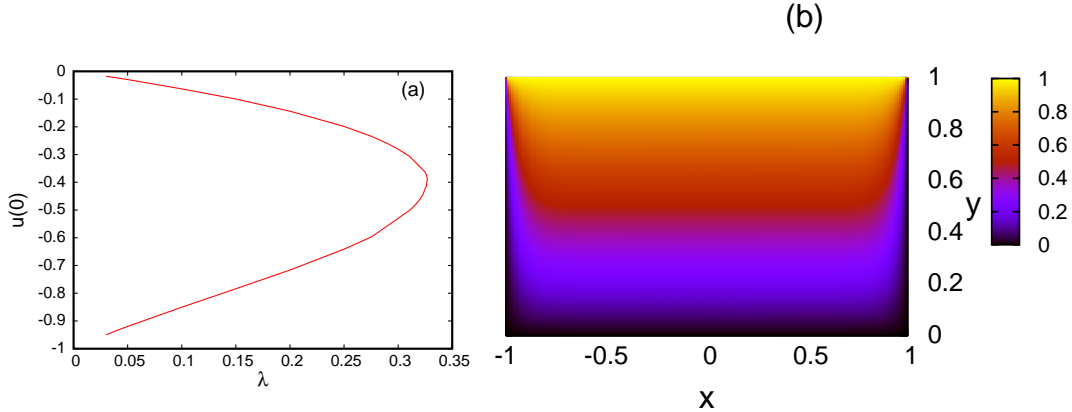


Figure 1: (Color online)  $\epsilon = 0.2$ . (a) Bifurcation diagram from numerical solution of steady equations (14) and (16). (b) contour plot of  $\phi$  for  $\lambda = 0.32$ .

A low initial guess for  $u'(-1)$ , between 0 and  $-1.5$ , resulted in the numerical solution for  $u$  converging to the upper branch of solutions and a high initial guess for  $u'(-1)$ , between  $-1.5$  and  $-3$ , resulted in convergence to the lower branch. For  $\epsilon = 0$ , it is known that  $\lambda_s^* = 0.350004\dots$  [5]. The numerical scheme was tested by finding  $\lambda_s^*$  in the limit  $\epsilon \rightarrow 0$  with  $\Delta x = \Delta \eta = 5 \times 10^{-3}$ . For  $\epsilon = 0.0001$  it was found that  $\lambda_s^* = 0.350000$ , which agrees with the value for  $\epsilon = 0$  to five decimal places, which is the accuracy for the critical  $\lambda$  which will be used in this work. The bifurcation curve for  $\epsilon = 0.2$  is shown in Figure 1(a). The bifurcation parameter chosen was the value of  $u$  at  $x = 0$ . Figure 1(b) shows a contour plot of the electric potential  $\phi$ . Due to  $\epsilon$  being small, over a large part of the domain the electric potential for the free boundary problem is close to the potential for the small aspect ratio limit (6), which in the transformed variables is  $\phi_0(x, \eta) = \eta$ .

## 2 Dynamical solutions

The dynamical behaviour of the membrane was also investigated, as discussed above for the small aspect ratio model (7). To investigate the dynamical behaviour of the membrane, the forced heat equation

$$u_t - u_{xx} = -\lambda \left[ \frac{1 + \epsilon^2 u_x^2}{(1 + u(x))^2} \right] |\phi_\eta(x, 1, t)|^2 \quad (17)$$

and the forced, damped wave equation

$$\gamma u_{tt} + u_t - u_{xx} = -\lambda \left[ \frac{1 + \epsilon^2 u_x^2}{(1 + u(x))^2} \right] |\phi_\eta(x, 1, t)|^2 \quad (18)$$



$\epsilon$	$\lambda_s^*$ static equation	$\lambda_h^*$ heat equation
0.01	0.34997	0.34996
0.1	0.34536	0.34535
0.2	0.32738	0.32736
0.3	0.29356	0.29353

Table 1: Critical values  $\lambda_s^*$  for stationary solution for steady equations (14) and (16) (second column) and  $\lambda_h^*$  obtained from the potential equation (14) and forced heat equation (17) (third column).

were solved for the membrane displacement  $u$ . As mentioned in the Introduction, we assume that the motion starts from rest. This means that the initial condition for the heat equation (17) is  $u(x, 0) = 0$ , while for the damped wave equation (18) we take  $u(x, 0) = 0$  and  $u_t(x, 0) = 0$ .

The forced heat equation (17) was solved using centred differences in space  $x$  and an Euler scheme in time  $t$ , resulting in an explicit scheme with error  $O(\Delta t)$  in time and error  $O(\Delta x^2, \Delta \eta^2)$  in space, the same spatial accuracy as the numerical scheme used to solve the potential equation (14) and which was discussed in the previous section. The same Picard iteration as discussed in the previous section was used to find  $\phi_\eta(x, 1)$  in the deformation equation (16). Except for the first time step, the value of  $\phi_\eta(x, 1)$  at the previous time step was used as the initial guess for the iteration. The potential equation (14) was again solved using Jacobi iteration. The solution for  $\phi$  at the previous time step was used as the initial guess, which resulted in fast convergence. The accuracy of the heat equation was again tested by finding the critical  $\lambda$  in the limit  $\epsilon \rightarrow 0$  as in this limit the heat equation must give the known value  $\lambda^* = 0.350004\dots$  [5]. For  $\epsilon = 0.0001$ ,  $\Delta t = 1 \times 10^{-5}$  and  $\Delta x = \Delta \eta = 5 \times 10^{-3}$  the critical value 0.350006 was found, which agrees with  $\lambda_s^*$  to five decimal places. Note that the electric potential now depends on time due to the time dependence of the coefficients of the elliptic operator  $\mathcal{L}_u$  defined in (15).

The forced, damped wave equation (18) was solved using centred differences in space  $x$  and time  $t$ , again resulting in an explicit scheme with error  $O(\Delta t^2)$  in time and  $O(\Delta x^2, \Delta \eta^2)$  in space, again the same spatial accuracy as the scheme used to solve the potential equation (14). The same Picard iteration as for the stationary solutions of the previous section and the solution of the heat equation was used to find  $\phi_\eta(x, 1)$  from the elastic equation (16) with the iteration started with the value of  $\phi_\eta(x, 1)$  at the previous time step, as for the heat equation. As for the heat equation, the potential equation (14) was solved using Jacobi iteration, as using the solution at the

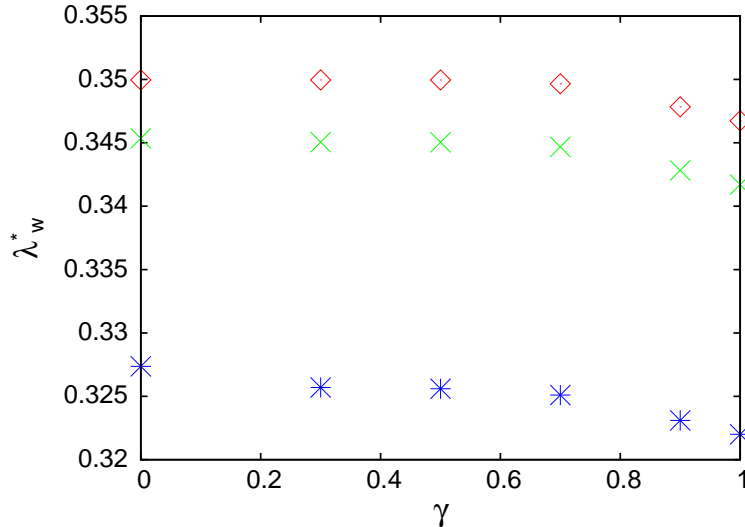


Figure 2: (Color online) Plot of the critical values of  $\lambda$  as a function of  $\gamma$  for  $\epsilon = 0.01$ : (red) diamonds,  $\epsilon = 0.1$ : (green) cross,  $\epsilon = 0.2$ : (blue) star.

previous time step as the initial guess resulted in fast convergence. The scheme was tested by decreasing the space and time steps until the critical values of  $\lambda$  did not change to five decimal places. It was found that  $\Delta t = 2 \times 10^{-3}$  and  $\Delta x = \Delta \eta = 5 \times 10^{-3}$  were sufficient for this.

The dependence of the critical value  $\lambda_s^*(\epsilon)$  for a steady solution  $u$  to exist is further illustrated in Table 1, with the dynamic critical values illustrated in Table 1 and Figure 2. The table and figure show the critical values  $\lambda_s^*$ ,  $\lambda_h^*$ , and  $\lambda_w^*$  as found from the steady equations (14) and (16), the potential equation (14) and the forced heat equation (17) for  $u$  and the potential equation (14) and the forced, damped wave equation (18) for  $u$ , respectively. As discussed above, the dynamical critical value  $\lambda_h^*$  as determined from the forced heat equation for  $u$  is slightly lower than the static value. However, the difference is so small and the monotonic in time behaviour of the membrane profiles  $u$  make us believe that the two critical values are equal. The monotonic approach of  $u$  to the steady state when the elastic deformation is governed by the forced heat equation is illustrated in Figure 3. Note that by  $t = 10$  the solution has reached the steady state. Note that in Figure 2 the values  $\lambda_h^*$  have been plotted as the points with  $\gamma = 0$ . To summarize the results, we have that for  $\epsilon > 0$ ,  $\lambda_w^*(\epsilon) < \lambda_h^*(\epsilon) = \lambda_s^*(\epsilon)$ . In the case  $\epsilon = 0$ , it is known that  $\lambda_h^* = \lambda^*$ , while the results of Flores [11] indicate that  $\lambda_w^* < \lambda^*$ .

The behaviour of the pull-in value is more involved when the displacement  $u$  is given by the damped, forced wave equation (18), as can be seen on comparing the critical

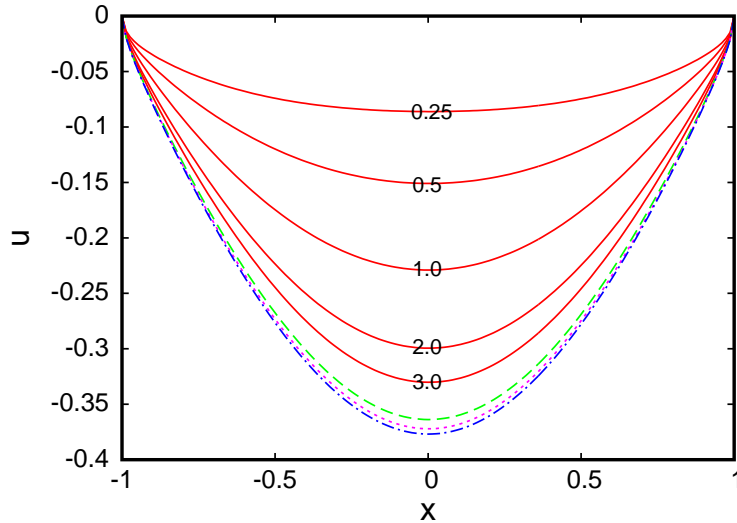


Figure 3: (Color online) Solution for  $u(x,t)$  for the potential equation (14) and the heat equation (17) for  $\epsilon = 0.2$  and  $\lambda = 0.327$ . The times  $t$  for each solution are on the solution curve, except for  $t = 6$ : green (long dash) curve,  $t = 8$ : pink (short dash) curve and  $t = 10$ : blue (dot-dash) curve.

values in Table 1 for the heat equation and Figure 2 for the damped wave equation, again noting that the values  $\lambda_s^*$  have been plotted as the points for  $\gamma = 0$  in Figure 2. For low values of the inertia  $\gamma$  the critical value  $\lambda_w^*$  is little changed from  $\lambda_h^*$ . This is to be expected as the damping  $u_t$  dominates the inertia term  $\gamma u_{tt}$  in the forced, damped wave equation (18) for small inertia coefficient  $\gamma$ . There is little change in the critical value  $\lambda_w^*$  for  $\gamma$  up to 0.5. Increasing the inertia  $\gamma$  to 0.7 results in a significant change in  $\lambda_w^*$  over  $\lambda_h^*$ , with the former value being lowered, as expected. The addition of inertia results in the membrane oscillating around the steady state, in a way that resembles the case of the overdamped spring model (1). The inertia is responsible for the lowering of  $\lambda_w^*$  with respect to  $\lambda_s^*$ , even in the limiting case of small aspect ratio  $\epsilon = 0$ , as reported by Flores [11]. However, the aspect ratio has a stronger effect on the lowering of  $\lambda_w^*$ .

The oscillatory approach of  $u$  to the steady state when the displacement  $u$  is governed by the forced, damped wave equation (18) is illustrated in Figure 4. The parameter values  $\lambda = 0.34$ ,  $\epsilon = 0.1$  and  $\gamma = 0.7$  were chosen so that the evolution is just below the critical  $\lambda_w^* = 0.34468$ . The evolution is shown until the steady state is reached by  $t = 10$ . The profile reaches a maximum depth for  $t \approx 3$  and then oscillates back up. Before this time, the profiles are monotonically increasing in depth. After  $t = 3$  the profiles monotonically decrease in depth until the steady state is reached. Thus, the behavior is similar to that of a heavily damped spring, as in the model (1) as

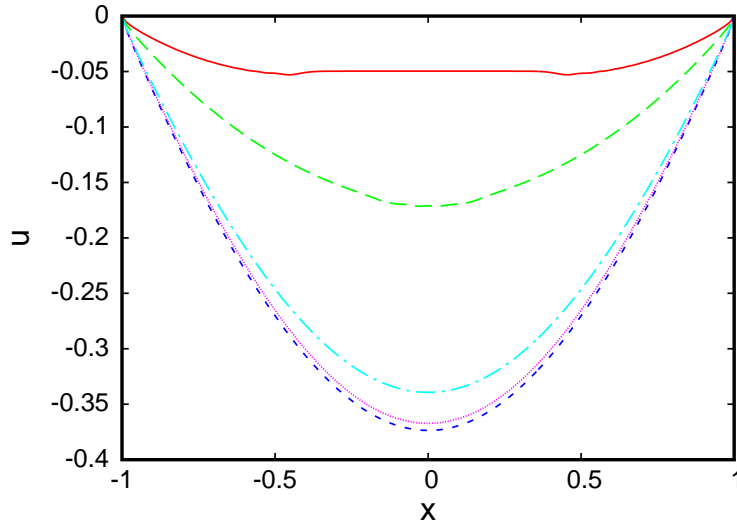


Figure 4: (Color online) Numerical solution of potential equation (14) and forced, damped wave equation (18) for  $\lambda = 0.34$ ,  $\epsilon = 0.1$  and  $\gamma = 0.7$ .  $t = 0.5$ : red (solid) line,  $t = 1.0$ : green (long dashed line),  $t = 3.0$ : blue (short dashed) line,  $t = 5.0$ : pink (dotted) line,  $t = 10.0$ : light blue (dot-dashed) line.

reported by Rocha *et al* [2].

The contrasting evolution when quenching occurs is illustrated in Figure 5. The parameter values were chosen just above the critical  $\lambda_w^* = 0.3251$ , with  $\lambda = 0.327$ ,  $\epsilon = 0.2$  and  $\gamma = 0.7$ . For these parameter values,  $\lambda_s^* = 0.32738$ . First, the profiles move on a fast time scale and approach the steady state corresponding to the static critical value. There is then a slow motion away from that steady state until the depth has increased far enough that the profiles can move on a fast time scale towards  $u = -1$ . This is similar to the observations of Rocha *et al* [2] for the model (1). Kavallaris *et al* [14] obtained oscillations around the steady state and later approach to touchdown for values of  $\lambda$  close to, but smaller than the critical static value. The oscillations are explained by the fact that their model corresponds to the regime in which inertial forces dominate. For our problem, in the third stage the displacement  $u$  rapidly approaches quenching, at which point the numerical solution breaks down.

### 3 Conclusions

The static and dynamical behaviour of a flexible membrane driven by an electric field in a MEMS device has been investigated. This evolution is governed by a potential equation for the electric field with a nonlinear boundary condition giving the membrane profile. This moving boundary problem was transformed into a boundary value

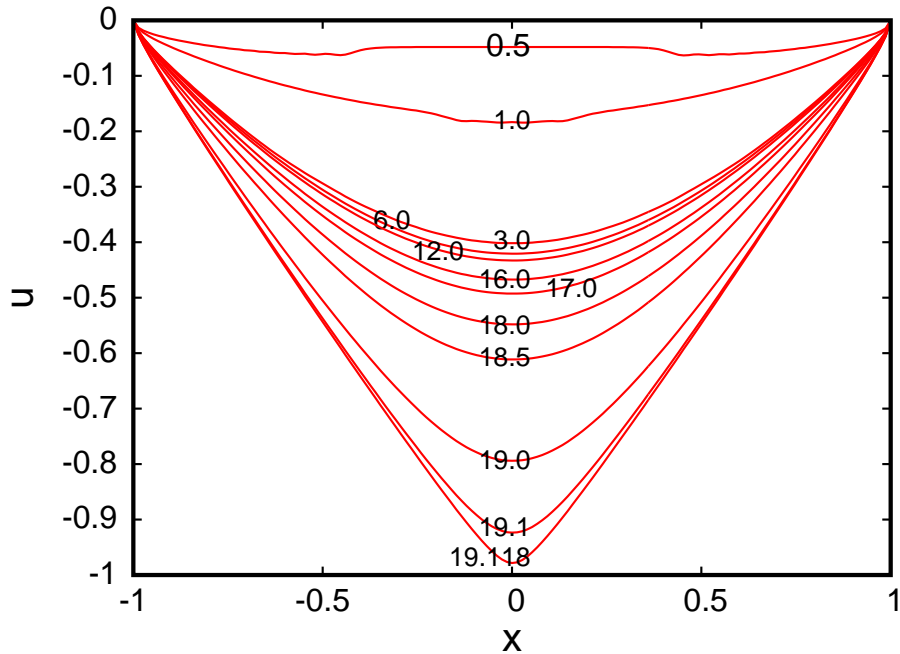


Figure 5: (Color online) Numerical solution of potential equation (14) and forced, damped wave equation (18) for  $\lambda = 0.327$ ,  $\epsilon = 0.2$  and  $\gamma = 0.7$ . The numbers on the curves are the time  $t$  for the solution.

problem on a fixed, rectangular domain, which was then investigated numerically due to the complexity of these equations. One of the findings is that the bifurcation curve has a single turning point with a shape which is qualitatively similar to that obtained in the limiting case of vanishing aspect ratio. The dynamical evolution of the membrane was investigated by replacing the static membrane equation with both a forced heat equation and a forced, damped wave equation. It was found that there is a critical value of the applied voltage for which the membrane does not settle to a steady state, but “quenches,” that is, it hits the bottom of the MEMS device, at which point the governing equations become invalid. In the case of the forced heat equation the dynamical critical value was found to be equal to the static critical value. In the case of the forced, damped wave equation, the dynamical critical value is lower than that for the static problem. The numerical results show that the dynamical and static critical values are different due to the inertial forces. However, the aspect ratio is more important in the determination of the dynamical critical value. This is due to the membrane oscillating in its evolution. These results show the increased complexity which arises from more realistic models of the MEMS device.

**Acknowledgments.** The financial support of CONACyT through Proyecto de Grupo 133036-F is gratefully acknowledged.

## References

- [1] A.V. Desai, J.D. Tice, C.A. Apblett and P.J.A. Kenis, “Design consideration for electrostatic microvalves with applications in poly(dimethylsiloxane)-based microfluidics,” *Lab Chip*, **12**, 1078–1088 (2012).
- [2] L.A. Rocha, E. Cretu and R.F. Wolffenbuttel, “Behavioural analysis of the pull-in dynamical transition,” *J. Microelectromech. Microeng.*, **14**, S37–S42 (2004).
- [3] W.-M. Zhang, H. Yan, Z.-K. Peng and G. Meng, “Electrostatic pull-in instability in MEMS/NEMS: A review,” *Sensors and Actuators A: Physical*, **214**, 187–218 (2014).
- [4] J.A. Pelesko and D.H. Bernstein, *Modelling MEMS and NEMS*, Chapman and Hall/CRC (2003).
- [5] G. Flores, G. Mercado, J.A. Pelesko and N.F. Smyth, “Analysis of the dynamics and touchdown in a model of electrostatic MEMS,” *SIAM J. Appl. Math.*, **67**, 434–446 (2007).
- [6] J.A. Pelesko and T.A. Driscoll, “The effect of the small-aspect-ratio approximation on canonical electrostatic MEMS models,” *J. Engng. Math.*, **53**, 239–252 (2005).
- [7] N.D. Brubaker, J.A. Pelesko, “Nonlinear effects on canonical MEMS models,” *Euro. Jnl. of Applied Mathematics*, **22**, 455–470, (2011).
- [8] A.E. Lindsay and M.J. Ward, “Asymptotics of some nonlinear eigenvalue problems for a MEMS capacitor: Part I: Fold point asymptotics,” *Meth. and Appl. of Analysis*, **15**, 297–326, 2008.
- [9] J. Wei and D. Ye, “On MEMS equation with fringing field,” *Proc. A.M.S.*, **138**, 1693–1699 (2010).
- [10] Z. Liu and X. Wang, “On a parabolic equation in MEMS with fringing field,” *Arch. Math.*, **98**, 373–381 (2012).

- [11] G. Flores, “Dynamics of a damped wave equation arising from MEMS,” *SIAM J. Appl. Math.*, **74**, 1025–1035 (2014).
- [12] P.H. Chang and H.A. Levine, “The quenching of solutions of semilinear hyperbolic equations,” *SIAM J. Math. Anal.*, **12**, 893–903, 1982.
- [13] R.A. Smith, “A quenching problem in several dimensions,” *SIAM. J. Math. Anal.*, **20** 1081–1094, 1989.
- [14] N.I. Kavallaris, A.A. Lacey, C.V. Nikolopoulos and D.E. Tzanetis, “A hyperbolic nonlocal problem modelling MEMS technology,” *Rocky Mountain J. Math.*, **41**, 505–534, 2011.
- [15] J.I. Siddique, R. Deaton, E. Sabo and J.A. Pelesko, “An experimental investigation of the theory of electrostatic deflections,” *J. Electrostatics*, **69**, 1–6 (2011).
- [16] P. Laurençot and C. Walker, “A stationary free boundary problem modeling electrostatic MEMS,” *Arch. Rational Mech. Anal.*, **207**, 139–158 (2013).
- [17] J. Escher, P. Laurençot and C. Walker, “A parabolic free boundary problem modeling electrostatic MEMS,” *Arch. Rat. Mech. Anal.*, **211**, 389–417 (2014).